

Estimates of multipolar coefficients to search for cosmic ray anisotropies with non-uniform or partial sky coverage.

Pierre Billoir^a & Olivier Deligny^b

^a*LPNHE (Universités Paris 6 & 7, CNRS-IN2P3), Paris, France*

^b*IPN (Université Paris Sud, CNRS-IN2P3), Orsay, France*

Abstract

We study the possibility to extract the multipolar moments of an underlying distribution from a set of cosmic rays observed with non-uniform or even partial sky coverage. We show that if the degree is assumed to be upper bounded by L , each multipolar moment can be recovered whatever the coverage, but with a variance increasing exponentially with the bound L if the coverage is zero somewhere. Despite this limitation, we show the possibility to test predictions of a model without any assumption on L by building an estimate of the covariance matrix seen through the exposure function.

1 Introduction

Anisotropy in the arrival directions of cosmic rays is a major observable to understand their origin. Magnetic fields bend their trajectories in such a way that transport of cosmic rays is mainly diffusive up to high energies: this makes their angular distribution isotropic. Nevertheless, above the so-called knee of cosmic rays up to the ankle, there are predictions for small but increasing anisotropies with energy, predictions which of course depend on the regular and the turbulent components of the assumed galactic magnetic field, as well as the assumed distribution of sources and composition of cosmic rays (Ptuskin et al. 1993; Candia et al. 2002). Further, at ultra-high energies, cosmic ray arrival directions are expected to be less and less smeared out by galactic and extragalactic magnetic fields, leading to a possible extraction of informations about the position of the sources (Isola et al. 2001; Sigl et al. 2003; Armengaud et al. 2005; Dolag et al. 2004; De Marco et al. 2006). Hence, it is clear that any evidence for an anisotropy, or any limit on anisotropies in the

cosmic ray locations observed by experiments are among the most important constraints upon models.

The multipole expansion up to a given order L is a powerful tool to study the structures standing out the noise down to an angular scale $\approx \pi/L$, whatever the shape of the underlying celestial pattern. In practice, the number of significant coefficients is limited by the angular resolution of the detector and, in the other hand, by the available statistics of observation. However, ground based experiments cover a limited range in declination, so that it is impossible to apply off the shelf the formalism of multipole moments: anyone of the coefficients may be modified in an unpredictable way by the unseen part of the sky. Methods have been developped to study the CMB with an incomplete coverage (Gorski 1994; Wright et al. 1994; Tegmark et al. 1996; Mortlock et al. 2002), but here we are faced to a different problem: we cannot suppose a priori that the distribution of cosmic rays is described by a power spectrum, because we want to detect possible non-isotropic structures, a priori unknown. In other terms, the information carried by the $a_{\ell m}$ cannot be reduced to the only knowledge of the C_ℓ .

One purpose of this paper is to study the possibility of estimating the multipole moments of a distribution of points over a sphere in case of a non-uniform or even a partial coverage of the sky, together with the limitations of such an approach. The estimation of dipoles and quadrupoles was studied in (Sommers 2001; Aublin & Parizot 2005; Roulet & Mollerach 2005). Here, we use the moments of the observed distribution on a set of orthogonal functions: either the spherical harmonics themselves, or a set of functions tailored on the coverage function. With these two different methods, we show that the interference between the modes induced by the the non-uniformity or the hole of the coverage can be removed assuming a bounded expansion in the conjugate space, allowing to recover the underlying multipole moments. However, in accordance with the simple intuition that it is impossible to describe the unseen part of the sky, we point out that the uncertainty on the recovered coefficients increases with the assumed bound L of the expansion. We show that the larger the hole in the coverage of the sky, the faster the increase of uncertainty with L . After some general considerations about the description of point processes on a sphere in Section 2, Sections 3 and 4 are dedicated to these methods whereas Section 5 illustrates them with some examples.

Because of the incomplete knowledge of the distribution of cosmic ray sources, and the stochastic nature of the propagation through magnetic fields, the anisotropies we want to characterize are not reducible to explicit models: they may be interpreted as a particular realization of a random process. This means that some model predictions are better expressed as average values of the coefficients, with their covariance matrix. This matrix is not necessarily diagonal to describe the physics we are interested in, contrary to the case of a power

spectrum. We show in Sect.6 that under reasonable assumptions, an estimate can be performed with a partial sky coverage, evading the problem of setting a bound to the expansion.

2 Generalities about point processes on a sphere

The number of cosmic rays $n(\theta, \varphi)$ observed as a function of $\Omega = (\theta, \varphi)$ is a random process that we can modelize with the following quantity :

$$n(\Omega) = \frac{1}{N} \sum_{i=1}^N \delta(\Omega, \Omega_i)$$

where δ is the Dirac function on the surface of the unit sphere, and Ω_i the position of the i^{th} cosmic ray. This distribution follows a Poisson law with an averaged density that we will denote by $\mu(\Omega)$:

$$\mu(\Omega) = \omega(\Omega)\lambda(\Omega).$$

Here, λ is the density of the distribution of cosmic rays and ω is the exposure function of the experiment. The multipole coefficients of the function $\lambda(\theta, \varphi)$ defined on the unit sphere express its expansion in spherical harmonics:

$$\lambda(\theta, \varphi) = \sum_{\ell, m} a_{\ell m} Y_{\ell}^m(\theta, \varphi) \quad (\ell \geq 0, \quad -\ell \leq m \leq \ell).$$

In this paper, we choose to normalize the spherical harmonics in such a way that $\int d\Omega Y_{\ell m}(\Omega) Y_{\ell' m'}(\Omega) = 4\pi \delta_{\ell \ell'} \delta_{m m'}$. Together with the normalization $\int d\Omega \lambda(\Omega) = 4\pi$, our convention leads to $a_{00} = 1$ which is, in the context of this study, a natural system of units. For convenience, we will use hereafter the notation $\sum_{\ell, m} = \sum_{\ell=0}^{\infty} \sum_{m=-\ell}^{\ell}$.

With a uniform sky coverage, it is easy to obtain an unbiased evaluation of these coefficients from a sample of N points (θ_i, φ_i) distributed independently according to the density λ :

$$\bar{a}_{\ell m} = \frac{1}{N} \sum_{i=1}^N Y_{\ell}^m(\theta_i, \varphi_i).$$

If the distribution is roughly uniform (that is, $|a_{\ell m}| \ll 1$ for all $(\ell, m) \neq (0, 0)$), these estimators are quasi-optimal, weakly correlated and their variances are

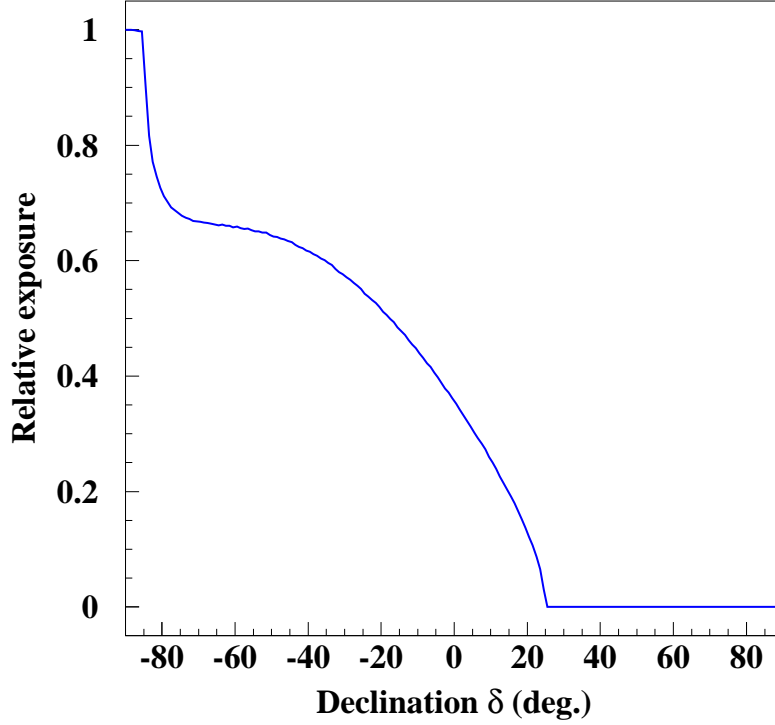


Fig. 1. *Relative exposure as a function of declination in equatorial coordinates of the Southern site of the Pierre Auger observatory. The detection efficiency is assumed to be saturated up to zenithal of 60° .*

close to $1/N$; otherwise the variances can be approximated from the quadratic moments:

$$\text{var}(\bar{a}_{\ell m}) = \frac{1}{N} \sum_i \left((Y_\ell^m(\theta_i, \varphi_i))^2 - (\bar{a}_{\ell m})^2 \right).$$

These properties are due to the orthogonality of the spherical harmonics, and cannot be used directly if the coverage of the sphere is not uniform, that is, if the distribution actually observed is $\lambda(\theta, \varphi)\omega(\theta, \varphi)$, where ω is a non-uniform function eventually vanishing in some regions.

However, if we suppose that the expansion of λ in spherical harmonics is bounded to degree L (at least in good approximation), we are going to see that it is possible to recover - within limitations that we will discuss in details - the multipolar coefficients even in case of partial sky coverage.

Throughout the paper, we will consider by default an exposure function not covering the whole sky in a realistic way since we use the function calculated by Sommers (Sommers 2001) describing the coverage of the sky of the Southern site of the Pierre Auger observatory as long as the acceptance of the detector is saturated until a local zenith angle θ_{\max} . This function is shown on Fig.1 with $\theta_{\max} = 60^\circ$, which guarantees in a realistic way this ideal function to be meaningful (Auger Collaboration 2005).

3 Estimate through the deconvolution of the exposure function

3.1 The estimate

In this section, we describe an estimate of the $a_{\ell m}$ coefficients based on the interpretation of the estimate

$$\bar{b}_{\ell m} = \frac{1}{N} \sum_{i=1}^N Y_{\ell}^m(\theta_i, \varphi_i)$$

in terms of a convolution between the underlying $a_{\ell m}$ coefficients of the density $\lambda(\theta, \varphi)$ and a kernel which depends on the $\omega(\theta, \varphi)$ function. In some extent, this approach is the equivalent of the MASTER one within the CMB framework (Hivon et al. 2002), except that we are interested here in building a linear estimate of the $a_{\ell m}$ coefficients rather than a quadratic estimate of the C_{ℓ} ones. As the cosmic rays are observed through the exposure function ω , the estimate $b_{\ell m}$ is not an estimate of the multipolar coefficients of the density λ , but an estimate of the multipolar coefficients of $\omega\lambda$. The $a_{\ell m}$ coefficients are thus related to the $b_{\ell m}$ ones through the following convolution

$$b_{\ell m} = \sum_{\ell', m'} [K]_{\ell\ell'}^{mm'} a_{\ell' m'}.$$

The kernel K is entirely determined by the specific exposure function. Indeed, by using the completeness relation of the spherical harmonics, the elements of the kernel $[K]_{\ell\ell'}^{mm'}$ read

$$[K]_{\ell\ell'}^{mm'} = \int_{4\pi} d\Omega Y_{\ell}^m(\Omega) \omega(\Omega) Y_{\ell'}^{m'}(\Omega).$$

This relation was referred to as the *convolution theorem* in (Peebles 1973), as this is the analog on the sphere of the convolution theorem for a Fourier's transform. Then, by using direct numerical results of K and K^{-1} for specific

exposure function ω , the underlying a_ℓ^m coefficients can be formally recovered through the following estimate

$$\bar{a}_{\ell m} = \sum_{\ell', m'} [K^{-1}]_{\ell \ell'}^{m m'} \bar{b}_{\ell' m'}.$$

3.2 Statistical properties of the estimate

The observed N points are sampled according to a Poissonian process on the sphere. Averaged over a large number of realisations of N events distributed according to $\mu(\theta, \varphi)$, it's elemental to compute the first and the second moment of $n(\Omega)$:

$$\begin{aligned} \langle n(\Omega) \rangle_P &= \mu(\Omega) \\ \langle n(\Omega) n(\Omega') \rangle_P &= \mu(\Omega) \mu(\Omega') + \mu(\Omega) \delta(\Omega, \Omega') \end{aligned}$$

where the subscript P stands for *Poisson*. The average of the $b_{\ell m}$ estimate then reads

$$\begin{aligned} \langle \bar{b}_{\ell m} \rangle_P &= \left\langle \int_{4\pi} d\Omega \, n(\Omega) Y_\ell^m(\Omega) \right\rangle_P \\ &= \int_{4\pi} d\Omega \, \mu(\Omega) Y_\ell^m(\Omega) \\ &= \sum_{\ell', m'} K_{\ell \ell'}^{m m'} a_{\ell' m'} \end{aligned}$$

leading to the following averaged $a_{\ell m}$ estimate

$$\begin{aligned} \langle \bar{a}_{\ell m} \rangle_P &= \sum_{\ell_1, m_1} [K^{-1}]_{\ell \ell_1}^{m m_1} \sum_{\ell_2, m_2} K_{\ell_1 \ell_2}^{m_1 m_2} a_{\ell_2 m_2} \\ &= \sum_{\ell_2, m_2} \sum_{\ell_1, m_1} [K^{-1}]_{\ell \ell_1}^{m m_1} K_{\ell_1 \ell_2}^{m_1 m_2} a_{\ell_2 m_2} \\ &= a_{\ell m}. \end{aligned}$$

Thus, it is clear that we have built an unbiased estimate. Turning to the covariance, we get in the same way

$$\begin{aligned} \text{cov}(\bar{b}_{\ell m}, \bar{b}_{\ell' m'}) &= \int_{4\pi} d\Omega d\Omega' \mu(\Omega) \mu(\Omega') Y_\ell^m(\Omega) Y_{\ell'}^{m'}(\Omega') \\ &\quad + \int_{4\pi} d\Omega d\Omega' \mu(\Omega) \delta(\Omega, \Omega') Y_\ell^m(\Omega) Y_{\ell'}^{m'}(\Omega') - \langle \bar{b}_{\ell m} \rangle_P \langle \bar{b}_{\ell' m'} \rangle_P. \end{aligned}$$

The only non vanishing term comes from the Poissonian part of the second moment of $n(\Omega)$:

$$\text{cov}(\bar{b}_{\ell m}, \bar{b}_{\ell' m'}) = \sum_{\ell_1, m_1} a_{\ell_1 m_1} \int_{4\pi} d\Omega Y_{\ell}^m(\Omega) Y_{\ell'}^{m'}(\Omega) \omega(\Omega) Y_{\ell_1}^{m_1}(\Omega).$$

Using the fact that we are in practice looking for small deviation per respect with isotropy as emphasized in the introduction (ie: $a_{\ell m}/a_{00} \ll 1$), this expression can be simplified to:

$$\text{cov}(\bar{b}_{\ell m}, \bar{b}_{\ell' m'}) = [K]_{\ell \ell'}^{mm'} a_{00},$$

leading to :

$$\text{var}(\bar{a}_{\ell m}) = [K^{-1}]_{\ell \ell}^{mm} a_{00}.$$

Let's remind that K being proportional to the number of events, the standard deviation of the reconstructed coefficients is hence proportional to $1/\sqrt{N}$ as expected. In case of a non-uniform *but full coverage* of the sky, the completeness relation of the spherical harmonics easily allows to give the following analytical expression of the K^{-1} operator :

$$[K^{-1}]_{\ell \ell'}^{mm'} = \int_{4\pi} d\Omega \frac{1}{\omega(\Omega)} Y_{\ell}^m(\Omega) Y_{\ell'}^{m'}(\Omega).$$

In case of partial coverage, the spherical harmonics are no longer orthogonal, in such a way that the coefficients of K^{-1} only satisfy the expression

$$\sum_{\ell_1, m_1}^L [O]_{\ell \ell_1}^{mm_1} [K^{-1}]_{\ell_1 \ell'}^{m_1 m'} = \int_{\Delta\Omega} d\Omega \frac{1}{\omega(\Omega)} Y_{\ell}^m(\Omega) Y_{\ell'}^{m'}(\Omega)$$

where $\Delta\Omega$ is the non-zero region of ω , and

$$[O]_{\ell \ell'}^{mm'} = \int_{\Delta\Omega} d\Omega Y_{\ell}^m(\Omega) Y_{\ell'}^{m'}(\Omega).$$

It is then obvious, in this latter case, that K^{-1} is invertible only if L is *finite*, and that the coefficients of K^{-1} strongly depend on the assumed bound L , leading to an indetermination of each coefficient as L is increasing. This indetermination is nothing else but the mathematical traduction that it's impossible to know the distribution of cosmic rays in the uncovered region of the sky.

4 Estimate through dedicated orthogonal functions

In this section, we describe another way, more intuitive, to recover the underlying $a_{\ell m}$ coefficients by applying the Gram-Schmidt procedure to the $\omega(\theta, \varphi) Y_\ell^m(\theta, \varphi)$ with $\ell \leq L$, which allows to build orthogonal functions from the coverage function. Then, by applying the formalism of moments to these functions; the $a_{\ell m}$ are obtained with linear combinations of these moments.

4.1 Applying the Gram-Schmidt procedure

The scalar product being defined as

$$\langle f | g \rangle = \frac{1}{4\pi} \int f^*(\theta, \varphi) g(\theta, \varphi) d\Omega,$$

the normalized spherical harmonics may be written as

$$Y_\ell^m(\theta, \varphi) = P_\ell^m(\cos \theta) e^{im\varphi}$$

where the P_ℓ^m are the associated Legendre functions supposed here to be normalized:

$$\frac{1}{2} \int_{-1}^1 P_\ell^m(x)^2 dx = 1.$$

In practical computations we use the real functions $Y_\ell^0(\theta, \varphi)$ for $m = 0$, and $\{\sqrt{2} P_\ell^m(\theta, \varphi) \cos(m\varphi), \sqrt{2} P_\ell^m(\theta, \varphi) \sin(m\varphi)\}$ for $1 \leq m \leq \ell$. For convenience we keep the notations with the Y_ℓ^m hereafter.

Let us suppose first that ω is a function of θ only (for example, if the coverage is uniform in right ascension). Then ωY_ℓ^m and $\omega Y_{\ell'}^{m'}$ are orthogonal if $m \neq m'$, and the orthogonalisation may be performed separately for each value of m , combining the ωY_ℓ^m with $m \leq \ell \leq L$. If $\mathcal{N}(f)$ represents the function f after normalization, we just need to set, for a given m :

$$\begin{aligned} Q_{|m|}^m &= \mathcal{N}(\omega P_{|m|}^m) \\ Q_{|m|+1}^m &= \mathcal{N}(\omega P_{|m|+1}^m - \langle Q_{|m|}^m | \omega P_{|m|+1}^m \rangle Q_{|m|}^m) \\ Q_{|m|+2}^m &= \mathcal{N}(\omega P_{|m|+2}^m - \langle Q_{|m|}^m | \omega P_{|m|+2}^m \rangle Q_{|m|}^m - \langle Q_{|m|+1}^m | \omega P_{|m|+2}^m \rangle Q_{|m|+1}^m) \\ &\dots \end{aligned}$$

$$Q_{|m|+p}^m = \mathcal{N}(\omega P_{|m|+p}^m - \sum_{k=0}^{p-1} \langle Q_{|m|+k}^m | \omega P_{|m|+p}^m \rangle Q_{|m|+k}^m) \\ \dots$$

Then the normalized functions Z_ℓ^m defined on the sphere by:

$$Z_\ell^m(\theta, \varphi) = Q_\ell^m(\cos \theta) e^{im\varphi}$$

are orthogonal to each other, and the subset of Z_ℓ^m with $|m| \leq \ell \leq L$ generates the same subspace as the ωY_ℓ^m with $|m| \leq \ell \leq L$. We can express them through a set of coefficients $C_{\ell\ell'}^m$:

$$Z_\ell^m(\theta, \varphi) = \sum_{\ell'=m}^{\ell} C_{\ell\ell'}^m \omega(\theta) Y_{\ell'}^m(\theta, \varphi).$$

If ω depends on both θ and φ , the same procedure can be applied, but the orthogonal functions are mixtures of different values of m , and there is no canonical way to obtain them; anyway it is possible to build a basis preserving the subset generated by $0 \leq \ell \leq L$ whatever L . For simplicity, we do not develop such a formalism here. In particular, as only a small dependence on φ is expected in the case we are interested in, it is possible to weight the events to account for this variation of the exposure as a function of the right ascension, and hence, the formalism applied here can be applied off the shelf.

To illustrate the method, Fig.2 displays the shape of the ωY_ℓ^m and the Z_ℓ^m , and the triangular matrix of transformation $C_{\ell\ell'}^m$ for $L = 15, m = 0$ (in logarithmic scale), in the case of the coverage function displayed in Fig.1. One can see that the off-diagonal terms (in absolute value) grow rapidly well above 1 with ℓ and dominate over the diagonal ones (the coefficients for other values of m have a quite similar pattern). This strong “mismatch” between the ωY_ℓ^m and the Z_ℓ^m is suggested by the shapes of the functions and may be understood qualitatively in the following way: for large values of $\ell - |m|$, the θ dependence of Y_ℓ^m has $\ell - |m|$ oscillations over the full interval $[0, \pi]$, while Z_ℓ^m has the same number of oscillations over the covered interval; this makes difficult a matching of Z_ℓ^m to functions like ωY_ℓ^m which have less oscillations over this interval.

4.2 Estimating the multipole coefficients

Points being distributed according to the density $\lambda(\theta, \varphi)$ (to be evaluated), and detected with a probability $\omega(\theta)$ (supposed to be known), the observed

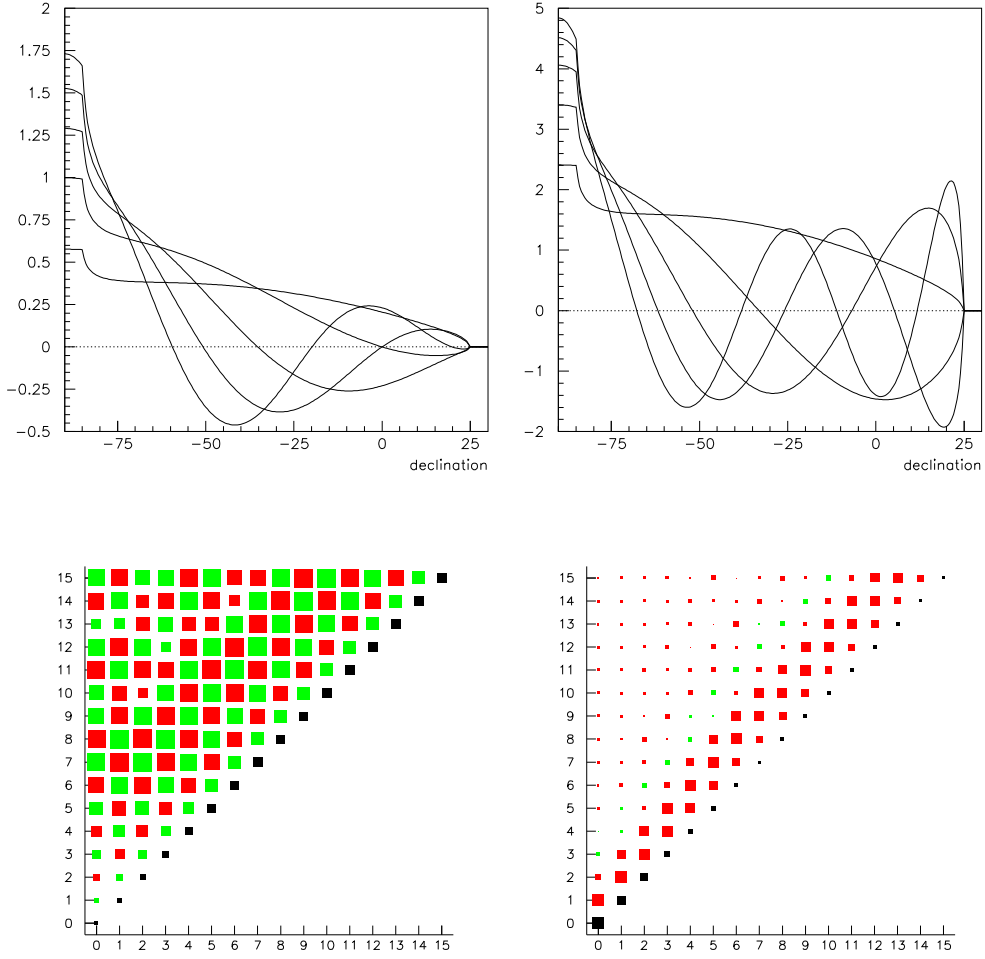


Fig. 2. Transformation between the ωY_ℓ^0 and the Z_ℓ^0 with the coverage function of Fig.1. Top: shape (as a function of the declination) for $\ell \leq 4$ (ωY_ℓ^0 on left side, Z_ℓ^0 on right side). Bottom: coefficients for $\ell \leq 15$; left: the $C_{\ell\ell'}^0$, in logarithmic scale: the area (in the units of the axes) is $\ln |C_{\ell\ell'}^0|/10$ (that is: a point represents 1, a unit square represents 2.2×10^4); the off-diagonal coefficients are in green if negative, in red if positive; right: the $D_{\ell\ell'}^0$ (inverse matrix) in linear scale 1:1, with the same sign convention.

points are distributed according to $\omega\lambda$: this function may be expanded over the Z_ℓ^m defined from ω as explained above:

$$\omega\lambda = \sum_{\ell,m} \alpha_{\ell m} Z_\ell^m$$

and an unbiased estimator of the $\alpha_{\ell m}$ is obtained from the points:

$$\bar{\alpha}_{\ell m} = \frac{1}{N} \sum_i Z_\ell^m(\theta_i, \varphi_i).$$

If λ is quasi-uniform, $\omega\lambda$ is almost proportional to Z_0^0 : the coefficient α_{00} is largely dominant. Then these estimators are quasi-optimal; if ω is not constant, the $\alpha_{\ell m}$, for a given value of m , may be correlated. If N is large, their covariance matrix is approximately given by quadratic moments:

$$\text{cov}(\bar{\alpha}_{\ell m}, \bar{\alpha}_{\ell' m}) \simeq \frac{1}{N} \sum_i Z_\ell^m(\theta_i, \varphi_i) Z_{\ell'}^m(\theta_i, \varphi_i) - \bar{\alpha}_{\ell m} \bar{\alpha}_{\ell' m}.$$

It is now easy to obtain estimators of the multipole coefficients of λ at a given order L by substituting the expressions of the Z_ℓ^m :

$$\omega\lambda \simeq \sum_{\ell, m}^L \bar{\alpha}_{\ell m} \sum_{\ell'=m}^{\ell} C_{\ell\ell'}^m \omega Y_{\ell'}^m,$$

that is:

$$\lambda \simeq \sum_{\ell, m}^L \bar{a}_{\ell m} Y_\ell^m \quad \text{with} \quad \bar{a}_{\ell m} = \sum_{\ell'=l}^L C_{\ell'\ell}^m \bar{\alpha}_{\ell' m}.$$

The $\bar{a}_{\ell m}$ with different values of m are not correlated, and the covariance matrix of the $\bar{a}_{\ell m}$ is given by:

$$\text{cov}(\bar{a}_{\ell_1 m}, \bar{a}_{\ell_2 m}) = \sum_{\ell', \ell''} C_{\ell'\ell_1}^m C_{\ell''\ell_2}^m \text{cov}(\bar{\alpha}_{\ell' m}, \bar{\alpha}_{\ell'' m}).$$

5 Illustrations

To illustrate the statistical properties of the estimates, we show here some simple applications of the methods in case of exposure shown on Fig.1. For the sake of clarity, we will refer to as *method 1* the method presented in section 3, and to as *method 2* the method presented in section 4.

5.1 Behaviour of variances with L

For illustrations, we use here the *method 1*. In a first time, we restrict the bound L to 1, so that we are interested here in research of a dipolar component only. We show on Fig.3 the reconstruction of the coefficient a_{10} in the case of an indeed dipolar distribution, whose excess of events points towards equatorial North with a magnitude $a_{10} = 0.1$. The red histogram drawn show

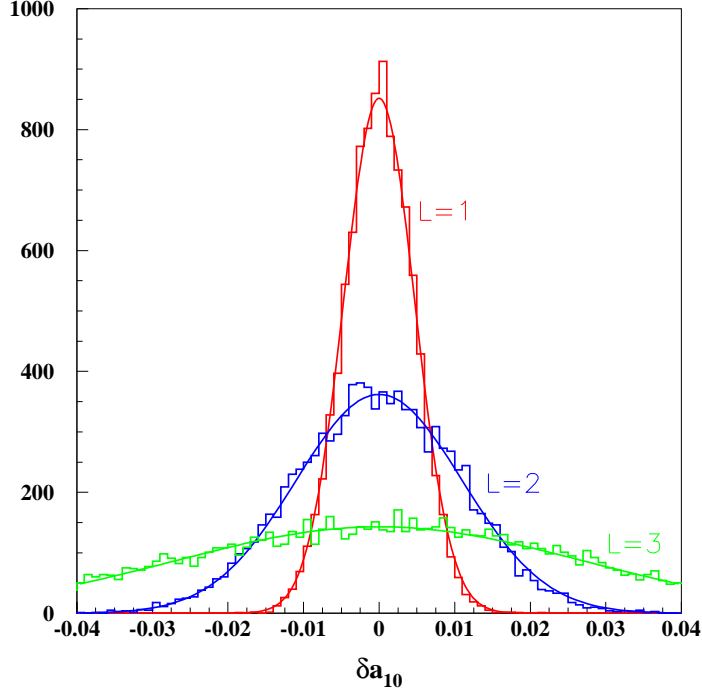


Fig. 3. *Reconstruction accuracy of the \bar{a}_{10} coefficient in case of a $a_{10} = 0.1$ dipolar pattern injected as a function of the assumed bound $L=1$ (red), 2 (blue), 3 (green), in case of exposure function shown on Fig.1. Histograms are from Monte-Carlo, and superimposed curves are Gaussian with averages and standard deviations from analytical predictions.*

the occurrence number of each reconstructed value of \bar{a}_{10} in case of $N = 10^5$ events generated by Monte-Carlo according to

$$\mu(\theta, \varphi) = \omega(\theta, \varphi)[1 + a_{10}Y_1^0(\theta, \varphi)].$$

Over the histogram is plotted a Gaussian curve whose average and standard deviation parameters are the ones determined in section 3.2. This curve matches the histogram, in such a way that the statistics previously determined by calculation describe the properties of the estimators indeed. Let us note that under the assumption of a purely dipolar distribution (ie $L=1$) the reconstruction of the multipolar coefficients is obtained in a very reasonable way.

Let us continue to illustrate the method by looking at the same multipolar coefficients, still in the case of a purely dipolar distribution, but by increasing the bound L to 2 and 3. Still on Fig.3, the blue and the green histograms and Gaussian curves plot the same quantities than the red ones but for $L = 2$ and $L = 3$ respectively, and illustrate the extremely fast degradation of the accuracy of the reconstruction of a_{10} by more than a factor 2 for each additional

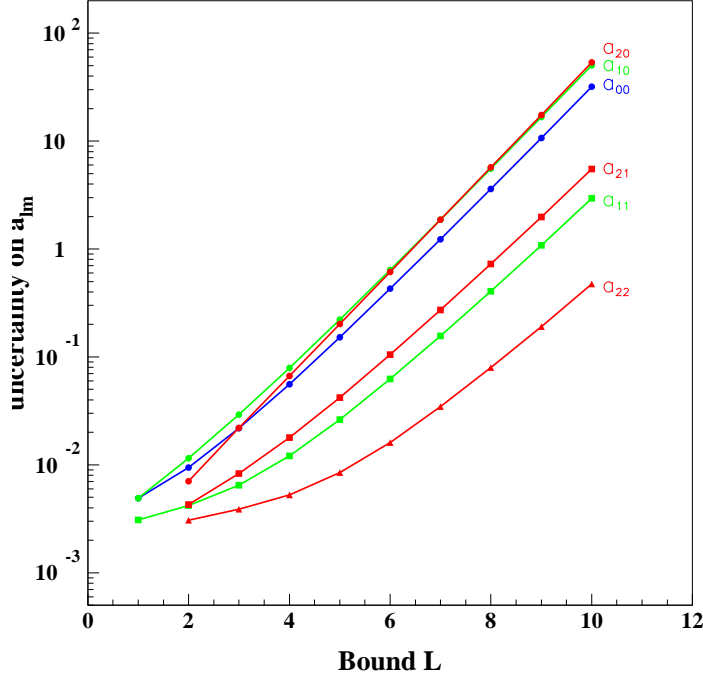


Fig. 4. Reconstruction accuracy of $\{a_{\ell m}\}_{\ell \leq 2}$ coefficients as a function of the assumed bound L , in case of exposure function shown on Fig.1. Increasing L leads to an explosion of the uncertainty on $a_{\ell m}$.

order.

This tendency to the widening of the laws is largely confirmed when one looks at the reconstruction of any coefficients $a_{\ell m}$ as a function of L . We show this property on Fig.4 for the $\{a_{\ell m}\}_{\ell \leq 2}$ set of coefficients, which illustrates clearly that it is increasingly difficult to give a meaning to the reconstructed values of the coefficients as soon as the maximum order of development is greater than 3.

5.2 Comparison of the two methods

Two samples of points were simulated according to a slightly anisotropic distribution ($a_{10}/a_{00} = 0.05$, $a_{1\pm 1} = 0$, i.e. dipole moment along z), multiplied by the coverage function drawn in Fig. 1; the $a_{\ell m}$ were estimated by both methods with the bound L going from 1 to 5. Fig. 5 shows that they give comparable results, and that the difference between them is generally smaller than the intrinsic difference between the samples (statistical fluctuations). Once again, one can see the divergence of the variances with increasing L .

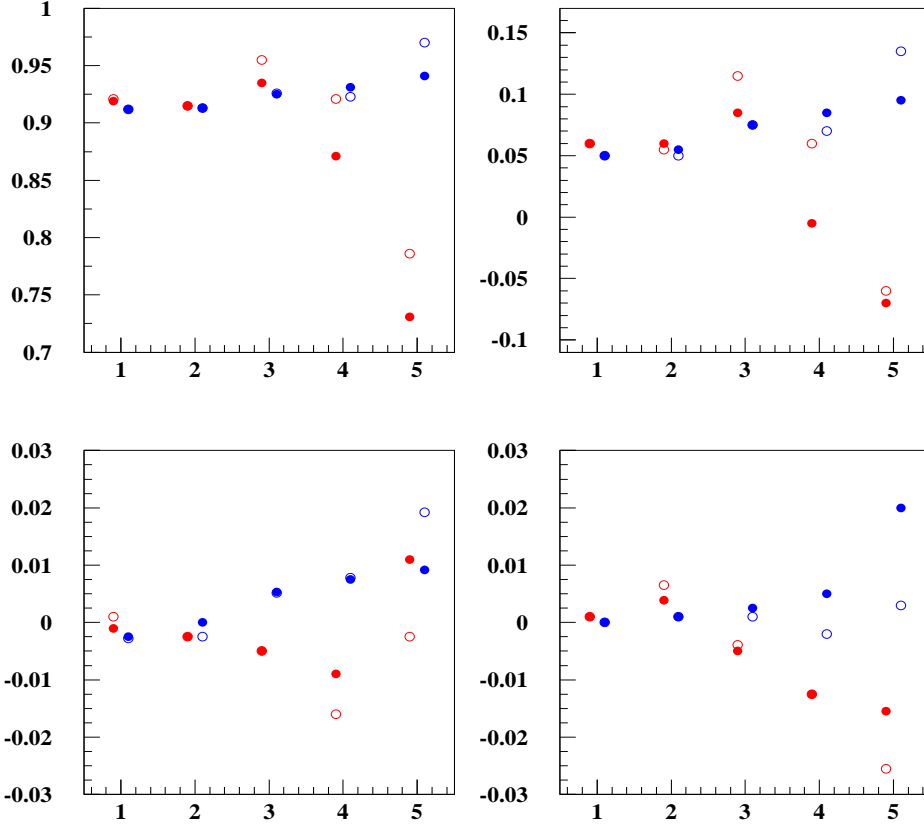


Fig. 5. Comparison of reconstructed coefficients $a_{\ell m}$ ($\ell = 0, 1$) on two simulated dipolar samples (red, blue) with the two methods (solid circles: method 1 presented in section 3; open circles: method 2 presented in section 4), with a bound L from 1 to 5. Top left: a_{00} ; top right: a_{10} ; bottom: a_{11} and a_{1-1} .

5.3 Highly non-uniform coverage of the whole sky

A contrario, with a complete coverage (even highly non-uniform), the size of the variance is stabilized at large L . This is illustrated in Fig. 6, comparing a partial coverage (cf Fig. 1) to this coverage completed by a small fraction of the same function in the opposite hemisphere, in such a way that there is no fully unseen region. Even a relatively small relative exposure in the Northern part of the sky allows to recover the coefficients with almost the same precision as if the exposure was uniform on the whole sky. Note however that if the exposure in the opposite hemisphere tends to zero, even if the phenomenon of stabilization at large L remains, the variance at any ℓ increases, tending towards a plateau determined roughly by $1/\sqrt{N'}$ where N' is in that case the total number of events which would be observed on the full sky through a

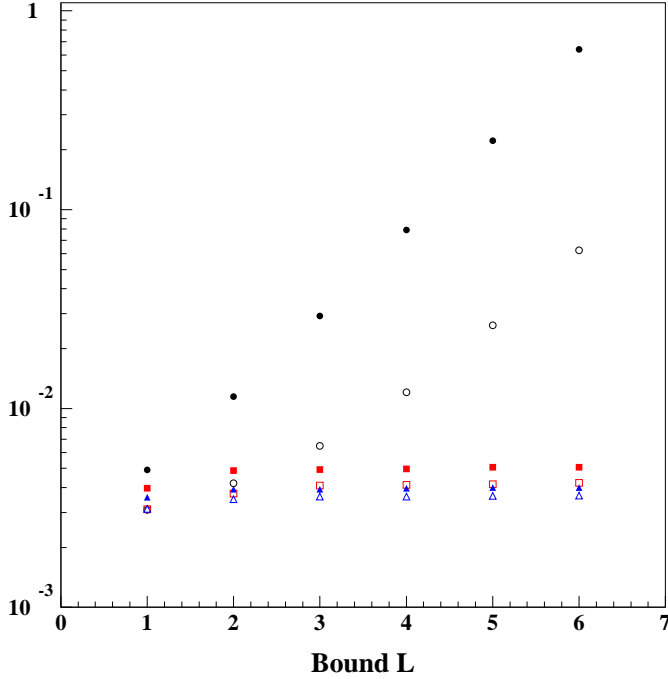


Fig. 6. *Dependence on the bound L of the variances of estimated $a_{\ell m}$ with a partial or a complete (but not uniform) coverage. Black circles: coverage function of Fig. 1; red squares: the same function plus 0.1 times the symmetric one w.r.t. the equatorial plane; blue triangles: the same + 0.2 times the symmetric one. The solid symbols correspond to a simulated dipolar distribution along z axis; the open ones correspond to a axis in the equatorial plane*

uniform window but with a low absolute coverage, in such a way that N' is small. Of course, the larger the size of the relative exposure tending to 0 is, the faster the increase of the variance towards this plateau occurs.

5.4 Angular distribution in the covered region

We have shown that using a large value of L in case of a partial coverage of the sky forbids to give to any $a_{\ell m}$ coefficient an interpretation of an individual multipolar moment. Nevertheless, one may wonder about the signification of the full set of coefficients $\{a_{\ell m}\}$. As a toy example, we generated a distribution of points according to the exposure function of Fig.1 times the function shown on Fig.7 (top left) which is a combination of Y_1^1, Y_2^2 and Y_3^1 . On top right of Fig.7, we show the reconstructed sky assuming L to be equals to 3, which illustrates that *the reconstructed sky matches the injected one in the covered region even if the variance on each reconstructed multipolar coefficient is already large (as shown in preceding sub-sections) for $L=3$* . Increasing the

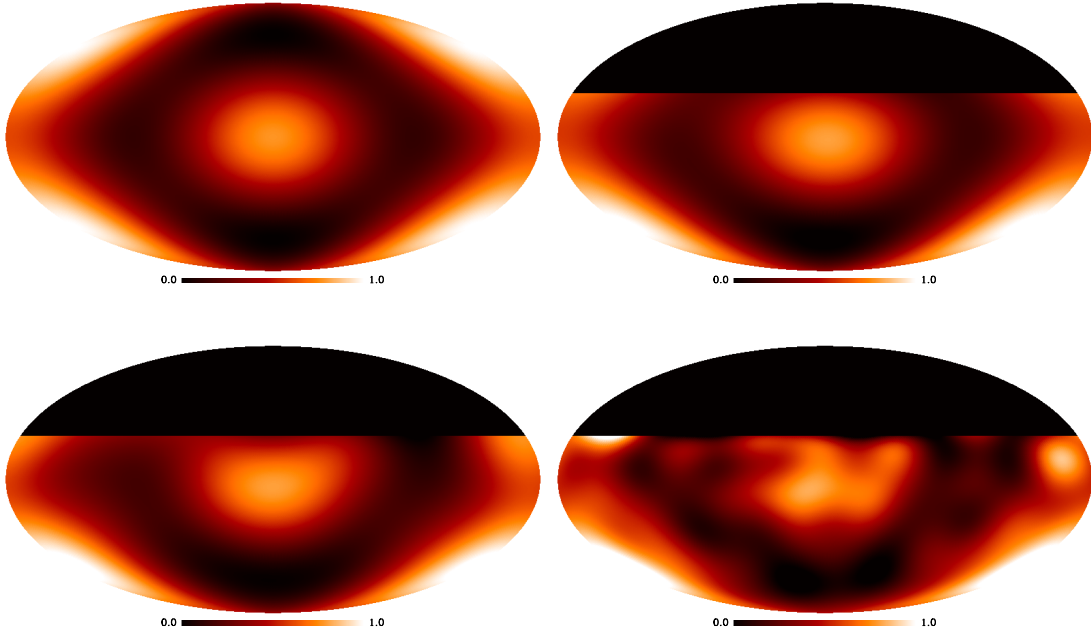


Fig. 7. *Top left: Toy injected sky (combination of Y_1^1, Y_2^2 and Y_3^1), in equatorial coordinates. Then recovered skies using different assumptions for L , and using the exposure function of Fig.1. Top right: Recovered sky assuming $L=3$. Bottom left: Recovered sky assuming $L=5$. Bottom right: Recovered sky assuming $L=10$. The unseen part of the sky is hidden.*

value of L to 5 (bottom left) or 10 (bottom right) do not change this property of the expansion, as only additional statistical fluctuations appear due to the finite number of points. On these plots, we hide the unseen part of the sky, where the reconstructed expansion is meaningless.

5.5 Hypothesis test

Any sky observed through an exposure function ω can thus be described precisely in the observed part of the sky by increasing L at a sufficient value. However the interpretation of each multipolar moment is problematic, because it depends strongly on the cut L . We want now to build a statistical test to obtain a reasonable value of L from the data themselves.

Starting from an hypothesis on L and the corresponding reconstructed $\{a_{\ell m}\}$ coefficients, the likelihood function \mathcal{L}_L built from the realization is

$$\mathcal{L}_L = \prod_{i=1}^N \left(\omega(\Omega_i) \sum_{\ell m}^L \bar{a}_{\ell m} Y_{\ell}^m(\Omega_i) \right).$$

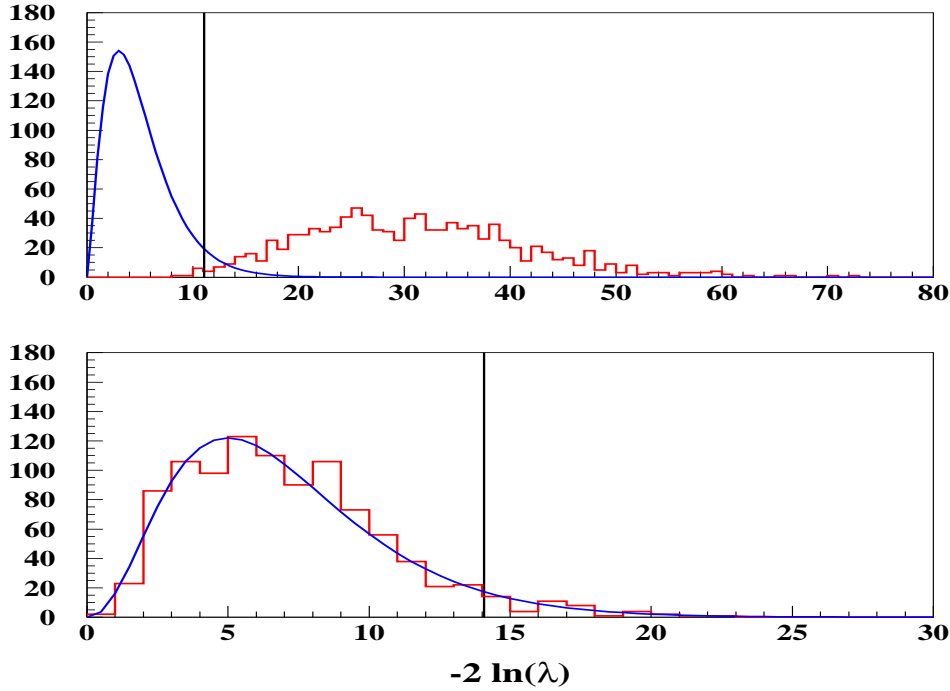


Fig. 8. Observed (red histograms) and expected (continuous blue line) distributions for λ in case of a quadrupolar injected pattern. Top: $L = 2$ against the null hypothesis $L=1$. Bottom: $L = 3$ against the null hypothesis $L=2$. The vertical line indicates the value of λ below which the null hypothesis is accepted with a threshold at 5%.

For any particular realization, from this likelihood (which depends on L), we apply the method of the likelihood ratio to accept or to reject (within some chosen threshold) a null hypothesis $H_0(\mathcal{L}_{L_0})$ with respect to another hypothesis $H_1(\mathcal{L}_{L_1})$ by computing

$$\lambda = \frac{\mathcal{L}_{L_0}}{\mathcal{L}_{L_1}}.$$

Asymptotically, for a sample obeying the hypothesis H_0 , $-2 \ln \lambda$ is distributed according to a χ^2 with a number of degrees of freedom equal to the number of extra parameters in the H_1 hypothesis with respect to H_0 . The value of λ for any particular realization can thus be used to validate (or to reject) an assumption on L .

As an example, let us assume that the cosmic rays follow a symmetrical quadrupolar distribution $1 + 0.1 \sin^2 \theta - 0.2 \cos^2 \theta$, and let us use once again the exposure function shown on Fig.1. By restricting the reconstruction to a dipolar distribution, one then finds an artefact amplitude of about 5%. To test the relevance of the hypothesis of a purely dipolar sky, one can thus - starting from this sky - estimate whether it is necessary or not to increase the degree

of the expansion by calculating the ratio of the likelihood between the null hypothesis $L=1$ and another hypothesis on L , $L=2$ for instance. To show the behavior of the test, we generated 1000 different realizations of the quadrupolar pattern with 100,000 points each, then we reconstructed the parameters of the expansion within the two hypotheses, and finally computed the ratio of likelihoods. In this case, the hypothesis $L = 2$ introduce 5 more parameters $\{a_{2m}\}$, and the expected values of $-2 \ln \lambda$ are asymptotically distributed as a χ^2 with 5 degrees of freedom. We plot the result on the top of Fig.8: by choosing the threshold of the test to be 5% (vertical line at $-2 \ln \lambda = 11.07$), only 8 realizations over 1000 are accidentally accepted (red histogram). On the contrary, repeating the same procedure to the $L=2$ null hypothesis with respect to the $L=3$ hypothesis, we show on the bottom of Fig.8 that the obtained distribution perfectly matches the asymptotical expected one (a χ^2 with 7 degrees of freedom in that case). With the same partial coverage, a similar test on samples of 1000 points gives a poor discrimination between different hypotheses, and with only 100 points the test is completely irrelevant.

This procedure may be used to define a “likely minimum value” L_{min} of L , and to prevent a wrong interpretation of multipolar coefficients obtained with a lower value, which are then biased (as the artefact dipole obtained above from a symmetric quadrupole). Of course, a given sample cannot provide by itself an absolute maximum for L , and in the presence of a hole the multipolar coefficients remain undefined without an external assumption; however let us point out that in many cases, the values of the coefficients at a given order have no intrinsic physical meaning if the distribution is of higher order.

6 Testing model predictions

Let us consider a distribution $\lambda(\theta, \varphi)$ with coefficients $a_{\ell m}$ on the Y_ℓ^m ; the observed distribution $\omega(\theta)\lambda(\theta, \varphi)$ has coefficients $\alpha_{\ell m}$ on the Y_ℓ^m , and the relation:

$$a_{\ell m} = \sum_{\ell'=\ell}^{\infty} C_{\ell'\ell}^m \alpha_{\ell' m}$$

may be inverted, because for each value of m the matrix $C_{\ell\ell'}$ is triangular, and the coefficients of the inverse relation may be computed exactly for any value of ℓ :

$$\alpha_{\ell m} = \sum_{\ell'=\ell}^{\infty} D_{\ell'\ell}^m a_{\ell' m}$$

The values of the $D_{\ell'\ell}^m$ are displayed in Fig.2 (right) with the same example as on the left plot, but in linear scale: contrary to the $C_{\ell'\ell}^m$, they remain below 1 in absolute value, and practically negligible far away from the diagonal¹.

As a consequence, if a model gives predictions about the $a_{\ell m}$, it will be possible, in some cases, to deduce predictions on the $\alpha_{\ell m}$, which can be tested without any assumption on L . In that sense, the compatibility of a model may be checked with observations over an incomplete sky with a precision depending on the available statistics (but, of course, it can never prove that this model is the only possible one).

If a model makes a deterministic prediction, comparing the $\alpha_{\ell m}$ to the predicted values may be a convenient way to test this model up to a given order of multipolarity, that is, down to a given angular scale. The method is potentially more interesting if the predictions are probabilistic. As we emphasized it in the introduction, this is a relevant framework to describe high energy cosmic rays physics. Indeed, even in a situation with a well-defined and structured configuration of sources, propagation of cosmic rays unavoidably leads to a probabilistic nature of the observable sky, that is to say, a probabilistic nature of the multipolar moments. Each class of models has intrinsically a natural variance encrypted in the $a_{\ell m}$ covariance matrix. Further, some models do not try to build a well-defined configuration of sources, but pick up randomly cosmic rays at sources according to some distributions, making even more impossible to circumvent the characterization of a particular data set through a relevant statistical tool.

Consequently, the discrimination of models through an exploratory search in a data set is potentially extremely powerful by looking for the distance of the full covariance matrix to the expected one. Most simple example is a model predicting random $a_{\ell m}$ following independent gaussian laws with variances σ_ℓ^2 . In that case, the covariance matrix for the $\alpha_{\ell m}$ reads

$$\text{cov}(\alpha_{\ell_1 m}, \alpha_{\ell_2 m}) = \sum_{\ell'=m}^{\infty} D_{\ell'\ell_1}^m D_{\ell'\ell_2}^m \sigma_{\ell'}^2$$

provided, of course, that this series converges: this is true if the series of σ_ℓ^2 converges (as it should do for physical models), and if the $D_{\ell'\ell_1}^m$ have the behaviour suggested by Fig.2.

¹ However, in practice, through the matrix inversion, the numerical divergence of the $C_{\ell'\ell}^m$ limits the expansion to $L \simeq 15$ for this kind of coverage function; this is sufficient for most studies on sky anisotropies.

7 Conclusions

To cope with a partial sky coverage, a formalism using the computation of moments on orthogonal functions was developed to recover the angular distribution of the incident flux from a sample of N observed points. If the multipolar expansion is assumed to be upper bounded by $\ell \leq L$, the coefficients $a_{\ell m}$ may be estimated with a variance proportional to $1/N$ as usually, with a penalty factor increasing exponentially with L if there is a hole in the coverage (but stabilizing rapidly if the coverage is nowhere vanishing, even highly non-uniform). Two methods were tested, giving similar results, and practically the same variances.

Statistical tests based on likelihood ratios may be built to check an hypothesis on the distribution, for example a given bound $\ell \leq L$. In any case, it is possible to express predictions of a model in terms of coefficients which can be computed without any assumption on L , and tested against the moments found with a sample of observed points.

The methods presented in this paper may be applied any cosmic ray dataset, provided that the arrival directions and the coverage of the sky are known within a reasonable precision.

Acknowledgments

We thank members of the Auger collaboration for helpful discussions. Fig.7 has been made using the HEALPix package (HEALPix).

References

- [Ptuskin et al. 1993] V. Ptuskin et al., *A&A* **268** (1993) 726
- [Candia et al. 2002] J. Candia et al., *JHEP* **12** (2002) 033, [astro-ph/0206336](#)
- [Gorski 1994] K. Gorski, *ApJL* **430** (1994) 85
- [Wright et al. 1994] E. L. Wright et al., *ApJ* **436** (1994) 443
- [Tegmark et al. 1996] M. Tegmark et al., *ApJ* **468** (1996) 214
- [Mortlock et al. 2002] D. Mortlock et al., *MNRAS* **330** (2002) 405
- [Isola et al. 2001] C. Isola & G. Sigl, *Phys.Rev.* **D66** (2002) 083002, [astro-ph/0203273](#).
- [Sigl et al. 2003] G. Sigl et al., *Phys.Rev.* **D68** (2003) 043002, [astro-ph/0302388](#).
- [Dolag et al. 2004] K. Dolag et al., *JCAP* **0501** (2005) 009, [astro-ph/0410419](#).
- [Armengaud et al. 2005] E. Armengaud et al., *Phys.Rev.* **D72** (2005) 043009, [astro-ph/0412525](#).
- [De Marco et al. 2006] D. De Marco et al., *JCAP* **0607** (2006) 015, [astro-ph/0603615](#).
- [Sommers 2001] P. Sommers, *Astropart.Phys.* **14** (2001) 271, [astro-ph/0004016](#).
- [Aublin & Parizot 2005] J. Aublin & E. Parizot, *A&A* **441** (2005) 407, [astro-ph/0504575](#).
- [Roulet & Mollerach 2005] E. Roulet & S. Mollerach, *JCAP* **0508** (2005) 004, [astro-ph/0504630](#).
- [Hivon et al. 2002] E. Hivon et al., *ApJ* 567 (2002) 2-17 [astro-ph/0105302](#).
- [Peebles 1973] P. J. E. Peebles, *ApJ* **185** (1973) 413-440
- [Auger Collaboration 2005] The Pierre Auger Collaboration, *Proc. of the 29th ICRC* (2005), [astro-ph/0511104](#)
- [HEALPix] K. M. Gorski et al. (1998), [astro-ph/9812350](#)